Nonlinear fishbone dynamics in spherical tokamaks

IOP Publishing | International Atomic Energy Agency Nuclear Fusion

Nucl. Fusion **57** (2017) 016034 (11pp) doi:10.1088/0029-5515/57/1/016034

Nonlinear fishbone dynamics in spherical tokamaks

Feng Wang[1,2], **G.Y. Fu**[1,3] **and Wei Shen**[4]

[1] Princeton Plasma Physics Laboratory, Princeton, NJ 08543, USA
[2] Key Laboratory of Materials Modification by Laser, Ion and Electron Beams (Ministry of Education), School of Physics and Optoelectronic Technology, Dalian University of Technology, Dalian 116024, People's Republic of China
[3] Institute for Fusion Theory and Simulation and Department of Physics Hangzhou, Zhejiang University, Hangzhou, 310027, People's Republic of China
[4] Institute of Plasma Physics, Chinese Academy of Science, Hefei 230031, People's Republic of China

E-mail: fu@pppl.gov

Received 20 April 2016, revised 7 October 2016
Accepted for publication 14 October 2016
Published 22 November 2016

Abstract

Linear and nonlinear kinetic-MHD hybrid simulations have been carried out to investigate linear stability and nonlinear dynamics of beam-driven fishbone instability in spherical tokamak plasmas. Realistic NSTX parameters with finite toroidal rotation were used. The results show that the fishbone is driven by both trapped and passing particles. The instability drive of passing particles is comparable to that of trapped particles in the linear regime. The effects of rotation are destabilizing and a new region of instability appears at higher $q_{\min}$ ($>$1.5) values, $q_{\min}$ being the minimum of safety factor profile. In the nonlinear regime, the mode saturates due to flattening of beam ion distribution, and this persists after initial saturation while mode frequency chirps down in such a way that the resonant trapped particles move out radially and keep in resonance with the mode. Correspondingly, the flattening region of beam ion distribution expands radially outward. A substantial fraction of initially non-resonant trapped particles become resonant around the time of mode saturation and keep in resonance with the mode as frequency chirps down. On the other hand, the fraction of resonant passing particles is significantly smaller than that of trapped particles. Our analysis shows that trapped particles provide the main drive to the mode in the nonlinear regime.

Keywords: NSTX, fishbone, frequency chirping, nonlinear dynamics, wave-particle interaction

(Some figures may appear in colour only in the online journal)

1. Introduction

Energetic particle physics is critical for understanding behaviours of burning plasma experiments such as ITER. Energetic particle-driven instabilities may degrade energetic particle confinement and alpha particle heating efficiency. Fishbone is one of the most important energetic particle instabilities and is commonly observed in many tokamaks and stellarators with neutral beam injection (NBI) heating and/or radio frequency (RF) heating. It was first observed in poloidal divertor experiments (PDX) with perpendicular neutral beam injection [1]. The instability was driven resonantly by energetic trapped beam ions with resonance condition $\omega = \omega_d$, where ω_d is the trapped particle's precessional drift frequency [2, 3]. The mode had strong downward frequency chirping, with magnetic signal evolution resembling the bones of a fish, and was thus named 'fishbone'. Since then fishbone instability has been observed in many tokamaks, spherical tori, and stellarators [4–11]. It has been shown that the instability can also be driven by passing energetic particles, in addition to trapped particles [12, 13].

In this paper, we focus on nonlinear dynamics of fishbone instability in spherical tokamak plasmas. Experimental studies showed that there exists low frequency and high frequency fishbone [14, 15]. In this study, the simulation results correspond to the low frequency fishbone. The 3D global kinetic/

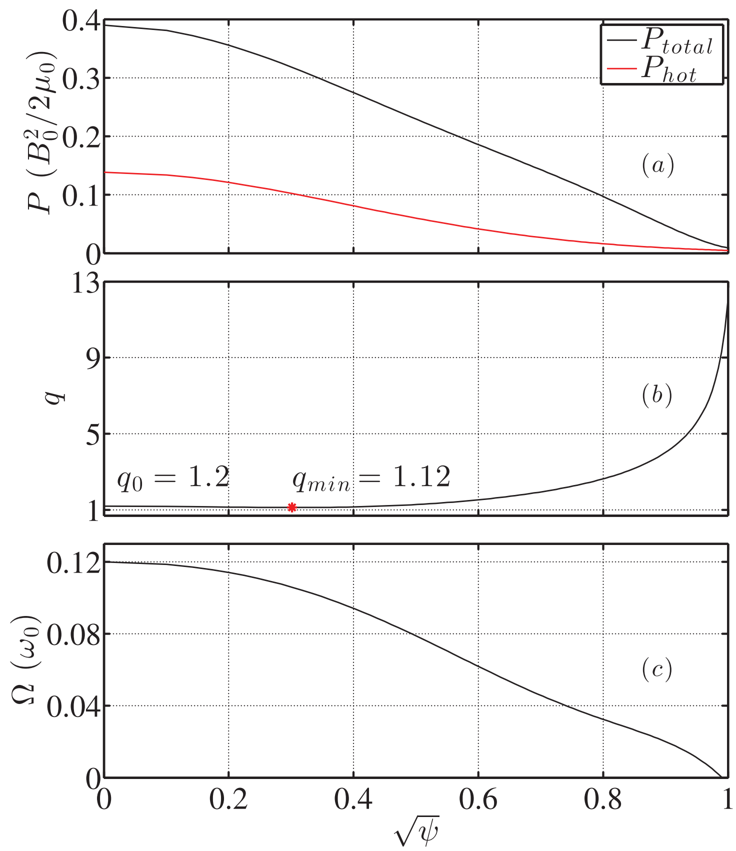

Figure 1. Equilibrium profiles versus $\sqrt{\psi}$: (*a*) total pressure P_{total}, energetic particle pressure P_{hot}, (*b*) safety factor q, (*c*) toroidal rotation Ω.

MHD hybrid code M3D-K [16, 17] is used to simulate beam-driven fishbone in this work. In M3D-K, the thermal plasma is described by the resistive MHD equations, while fast ion species are treated by the drift-kinetic equations. The fast ion pressure tensor P_h is coupled to the momentum equation. The system of hybrid equations are solved numerically as an initial value problem in toroidal geometry. The MHD equations are solved by the finite element method, and the drift-kinetic equations are solved by particle-in-cell method. The code has successfully been used to simulate internal kink mode, sawteeth, fishbone, toroidal Alfvén eigenmode, reversed shear Alfvén eigenmode, and tearing mode with effects of energetic particles [18, 19], [22–29].

Recently, the M3D-K code was used to study the linear stability and nonlinear dynamics of both non-resonant kink mode (NRK) and fishbone in NSTX plasmas with weakly reversed shear q profile and zero rotation [32, 33]. It was shown that the fishbone saturates with strong downward frequency chirping and flattening of beam ion distribution. In this work, we extend the previous study to include the effects of finite toroidal plasma rotation. More importantly, the detailed nonlinear wave particle interaction is investigated in order to understand the mechanism of frequency chirping and beam ion redistribution.

The paper is organized as follows. In the next section, the main parameters and profiles of our simulations are described. In section 3, we present simulation results of fishbone instability and wave particle resonances in linear phase. In section 4, we present the analysis of the nonlinear dynamics of fishbone including mode nonlinear evolution, frequency chirping, and nonlinear behaviors of wave particle interaction, and compare our results with the Berk–Breizman hole/clump theory [30, 31]. In section 5, we summarize our main results.

2. Equilibrium profiles and fast ion parameters

This work extends the previous work [32, 33] of $n = 1$ mode simulation in NSTX to include the effects of finite toroidal rotation and detailed analysis of nonlinear fishbone dynamics. The simulations in this study are also based on profiles and parameters of NSTX discharge 124379 at $t = 0.635$ s. The profiles of pressure, energetic particle pressure, safety factor (q) and toroidal rotation are shown in figure 1, where $\epsilon \equiv a/R_0 = 0.701$, $B_0 = 0.44$ T, and $\omega_0 = v_A/R = 8.246 \times 10^5$ rad s^{-1}. The rotation profile and amplitude are chosen according to the experimental data with $v_{\phi,0} = 8.5 \times 10^4$ m s^{-1}. In the NSTX experiment, the beam power was 4 MW, the total plasma beta was $\beta_t \equiv 2\mu_0 P_{\text{thermal+beam},0}/B_0^2 = 0.39$, beam ion beta $\beta_h \equiv 2\mu P_{\text{beam},0}/B_0^2$ and $\beta_h/\beta_t = 0.28$. The fast ion distribution is slowing down in energy, with a peaked distribution in pitch angle parameter:

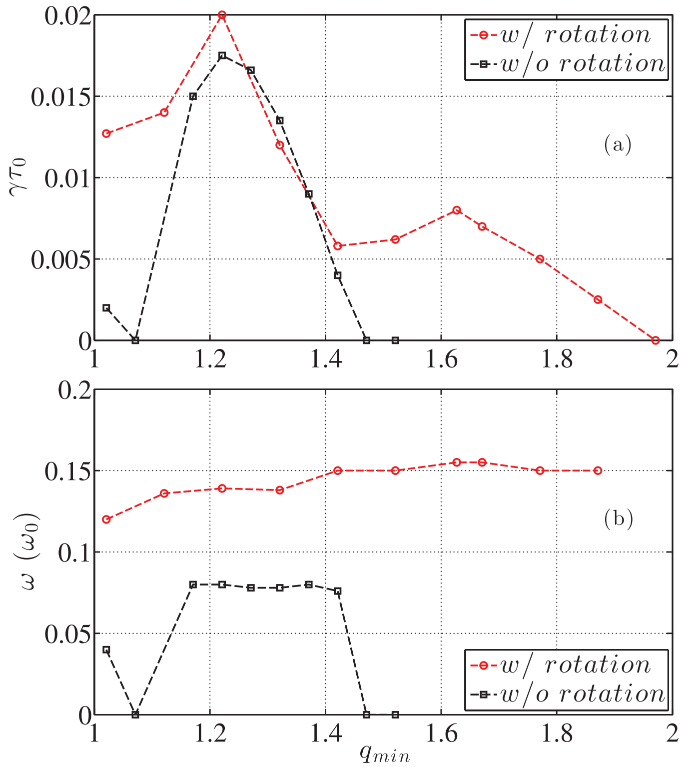

Figure 2. Linear growth rate (*a*) and mode frequency (*b*) versus $q_{\rm min}$ with and without rotation, $\beta_h/\beta_t = 0.35$.

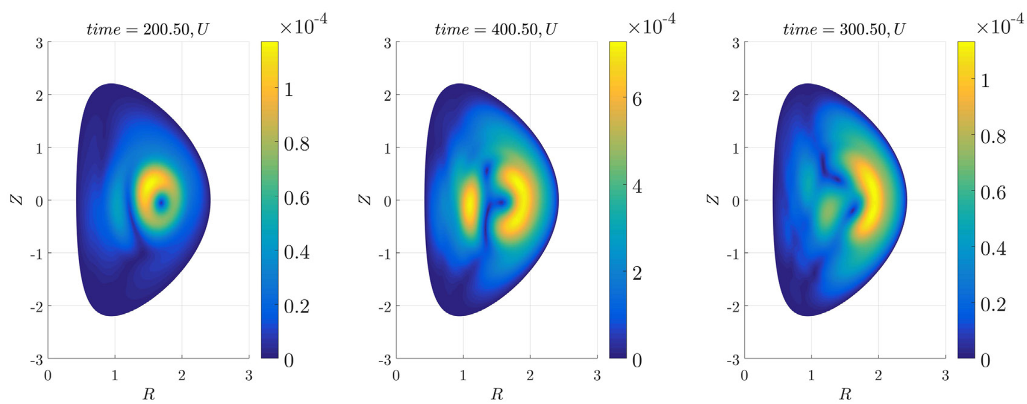

Figure 3. Linear mode structure (stream function U) with $q_{\rm min} = 1.021$, 1.321 and 1.621.

$$F_0 = \frac{cH(E_{\rm max} - E)}{E^{3/2} + E_c^{3/2}} {\rm e}^{-\frac{(\Lambda - \Lambda_0)^2}{\Delta\Lambda^2}} {\rm e}^{-\frac{\langle\psi\rangle}{\Delta\psi}}, \quad (1)$$

where c is a normalization factor, H is the step function; $E = v^2/2m_i + e\Phi$, where e is the particle charge and ϕ is the electric potential associated with the plasma rotation. $E_{\rm max} = v_0^2 m_i/2 + e\Phi$, where v_0 is the beam particle injection speed, and $E_c = v_c^2 m_i/2 + e\Phi$, where v_c is the critical velocity given by $v_c^3 \equiv 3\sqrt{\pi}\, m_e(2T_e/m_e)^{3/2}/m_i$, $\Lambda \equiv \mu B_0/E$ is the pitch angle parameter, where μ is the magnetic moment. ψ is normalized poloidal flux, and $\langle\psi\rangle$ is ψ averaged over particle orbit. The NBI injection energy of NSTX is 80 keV, the central pitch angle parameter $\Lambda_0 = 0.6$, and $\Delta\Lambda = 0.3$, $\Delta\psi = 0.3$. Note that these parameters are estimated based on the results of the beam ion code NUBEAM [34]. For simplicity, we only keep the $n = 1$ component of perturbation in the simulations discussed below, where $n = 1$ is the toroidal mode number, and simultaneously, we retain all poloidal harmonics for both linear and nonlinear studies. We also ignore the rotation effects on equilibrium due to low ratio of rotation velocity to ion thermal velocity. The energetic particles are described using the drift-kinetic equation with the δf particle-in-cell method; sources and sinks are not included

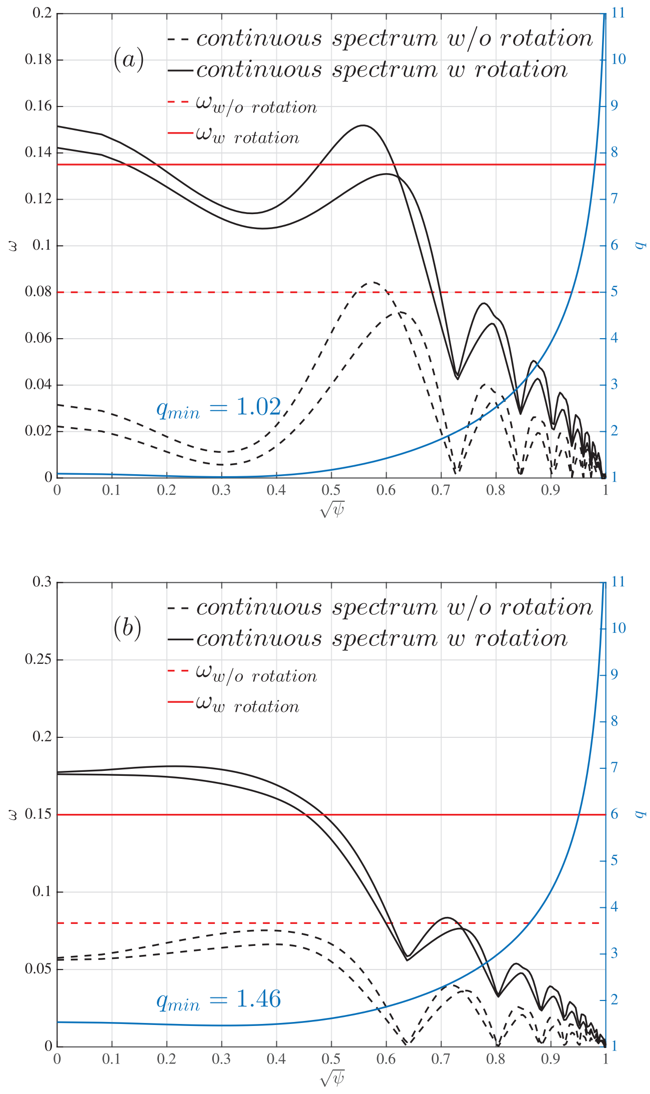

Figure 4. Continuous spectrum from NOVA with $q_{\min} = 1.02$ and $q_{\min} = 1.46$.

in the simulations. The thermal plasma is described using the extended MHD equations.

3. Linear simulation results

Linear simulations of beam-driven fishbone have been carried out based on parameters and profiles given above. In particular the effects of finite plasma rotation neglected in the previous work are included. In this study, the effects of the equilibrium component of v_ϕ are retained in the system of hybrid equations including the momentum equation and Ohm's Law. The static electric field associated with the toroidal rotation is included in the drift-kinetic equation for energetic particles. The rotation profile and amplitude are chosen according to the experimental data with $v_{\phi,0} = 8.5 \times 10^4$ m s^{-1} at the magnetic axis.

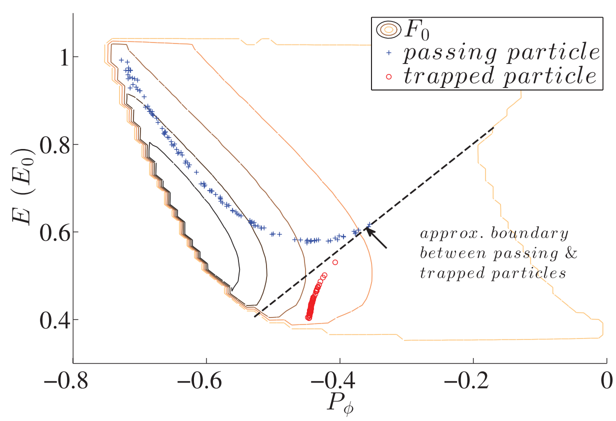

Figure 5. Unperturbed distribution function F_0, and linear resonant particle location in P_ϕ and E space, with $q_{\min} = 1.321$, $\beta_h/\beta_t = 0.2$ and $\mu \simeq 0.467$.

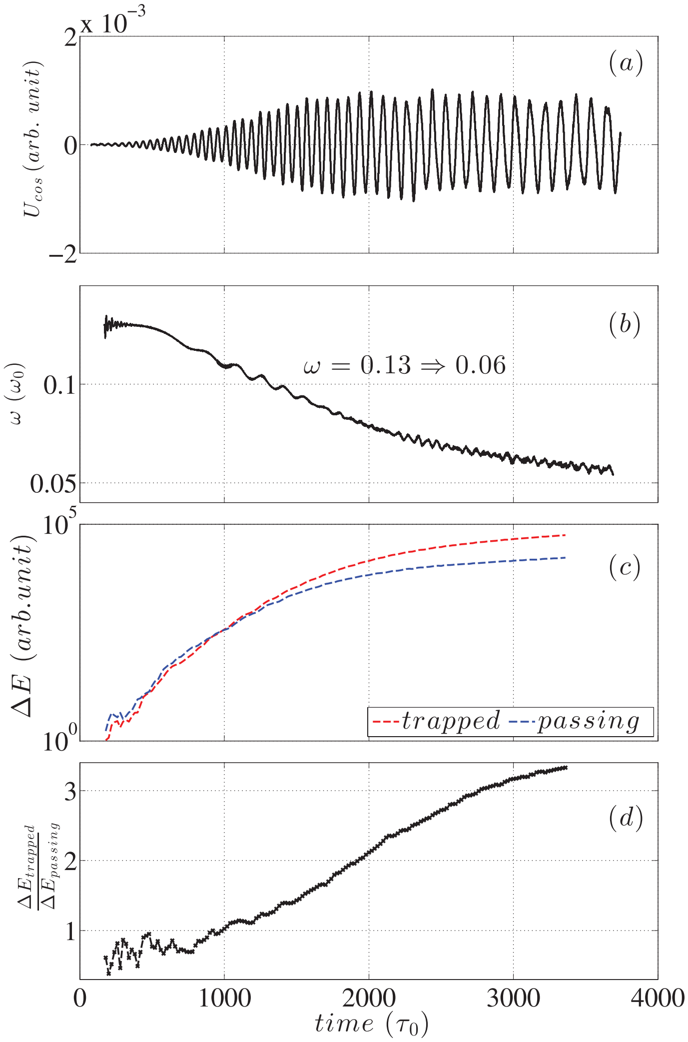

Figure 6. Nonlinear evolution of the fishbone mode: (*a*) *cos* component of U, (*b*) mode frequency, (*c*) energetic particles energy contribution from trapped and passing particles, (*d*) ratio of trapped particles' to passing particles' energy contribution.

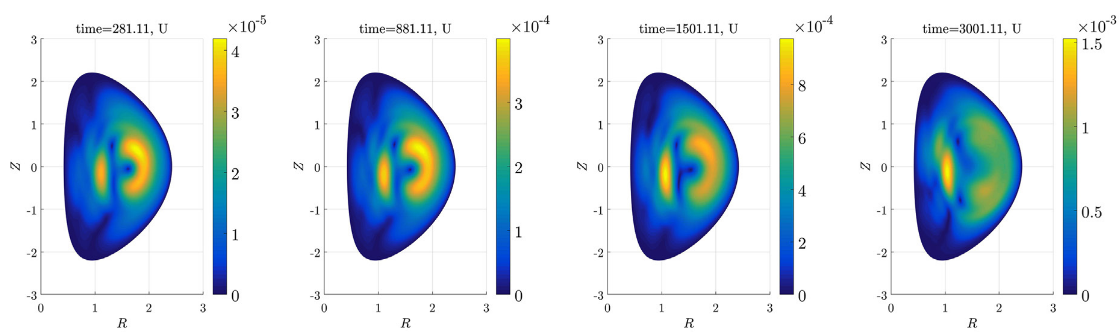

Figure 7. Amplitude of velocity stream function U in nonlinear evolution, R, Z are normalized by minor radius.

Figure 2 shows the growth rate ($\gamma\tau_0$) and mode frequency (ω) as a function of $q_{\min}$ at $\beta_h/\beta_t = 0.35$, where $\tau_0 = R/v_A = 1.2\ \mu$s. Note that in this $q_{\min}$ scan, the q profile is shifted up and down with its shape kept fixed. We observe that effects of rotation are destabilizing. Specifically, a new unstable region at higher $q_{\min}$ values appears due to the toroidal rotation. Figure 3 shows the linear mode structures with $q_{\min} = 1.021$, 1.321, and 1.621. It indicates that with $q_{\min} \simeq 1$, the mode is dominated by $m/n = 1/1$ component, and with higher $q_{\min}$, the mode is dominated by $m/n = 2/1$ component and has a ballooning

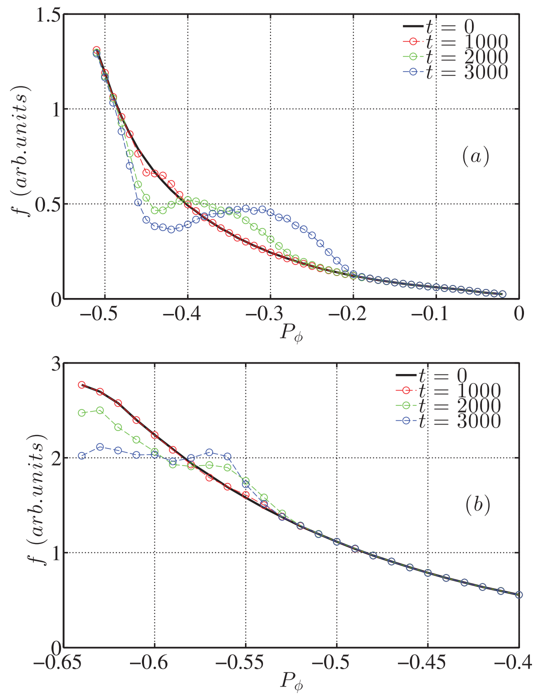

Figure 8. Distribution function in nonlinear evolution with $\mu \simeq 0.467$, (*a*) trapped particles with $E \simeq 0.406$ (E_0), (*b*) passing particles with $E \simeq 0.636$ (E_0).

structure. This result is similar to the appearance of m/n = 2/1 mode at higher $q_{\min}$ values in DIII-D plasmas [20].

It is not totally clear why rotation destabilizes fishbone at high $q_{\min}$. The sheared rotation can affect mode structure, beam ion drive and continuum damping. It can also affect beam ion resonance condition with finite orbit width. The sheared rotation can also affect the MHD stability. In order to better understand the sheared rotation effects on fishbone instability, figure 4 shows the low-frequency part of the sound-Alfvén continuous spectrum obtained using the ideal MHD code NOVA [21]. Clearly the continuous spectrum is significantly changed due to the finite sheared toroidal rotation. Therefore the sheared rotation can affect the fishbone stability via its effects on mode structure, beam ion drive and continuum damping. The detailed parameter dependence and physics of the rotational effects on fishbone will be investigated in future.

Note that in the actual experiment, there was no fishbone instability observed in this particular discharge around time = 0.635 s. Instead, the dominant mode was a neoclassical tearing mode (NTM) [22]. One reason is that our simulation model does not include the key NTM physics, which is important in this case. Another reason is that the instability is sensitive to the q and fast beam ion pressure profiles. With lower $q_{\min}$, the fishbone is stable—instead, the NRK mode is unstable in simulation, which may trigger NTM. Typically, in NSTX plasmas, fishbone's initial frequency in plasma frame is 8–10 kHz, and the chirping time is ≃3 ms (discharge #138872, time = 0.43–0.46 s) [35]. This is consistent with the simulation results, where the frequency is $\omega = 0.07\omega_0 = 9.19$ kHz, and the chirping time is ≃3.5 ms. For NRK, the mode frequency in plasma frame is very small as compared to that of the fishbone.

The instability drive of the fishbone is analyzed. In general, the mode is excited by free energy associated with radial gradient of beam ion distribution via wave particle resonant interaction. The resonance condition is given by

$$\omega = n\omega_\phi + p\omega_\theta, \qquad n,\ p \in \mathbb{Z} \tag{2}$$

where p is an integer. For passing particles, ω_θ and ω_ϕ are particle poloidal and toroidal transit frequencies respectively. For trapped particles, ω_θ is the bounce frequency and $\omega_\phi \equiv \omega_d$ is the toroidal precession drift frequency. For typical parameters it is found that main resonances are $p = 0$ and $p = 1$. Figure 5 plots $p = 0$ (red circles) and $p = 1$ (blue cross) resonant locations in the phase space of (E, P_ϕ) as well as contours of unperturbed beam ion distribution (F_0) at fixed value of magnetic moment $\mu \simeq 0.467$ (normalized by E_0/B_0). The value of magnetic moment is in the range of [0.0, 1.3]. The selected value of $\mu = 0.467$ is a typical one which contains a substantial region of both trapped and passing resonant particles. It is chosen to clearly illustrate the effects of both trapped and passing particles. However, the relative contribution of trapped and passing particles to the mode instability drive is calculated for whole phase space, not only for $\mu = 0.467$.

Note that the maximum energy of particles is a little larger than the injection energy ($E_{\max} = 1.03\ E_0$) due to the electric potential induced by the toroidal rotation. $P_\phi = e\psi + mv_\parallel RB_\phi/B$ is the toroidal angular momentum, here we use the code unit for P_ϕ, ψ denotes the poloidal flux in code units with $\psi = \psi_{\min}$ at the magnetic axis and $\psi = \psi_{\max} = 0$ at the plasma edge, which means for a fixed E, small P_ϕ corresponds to the plasma core, and large P_ϕ corresponds to the plasma edge. The approximate boundary between passing particles and trapped particles is indicated by the black dashed line. It is clear that $p = 0$ corresponds to precessional resonance of trapped particles and $p = 1$ corresponds to parallel resonance of passing particles.

Furthermore, the relative contribution of trapped particles and passing particles to the fishbone drive is estimated by calculating each particle's energy change at the end of the linear simulation. It is found that passing particles' destabilizing contribution is comparable to that of the trapped particles. For the specific case of $q_{\min} = 1.321$ and $\beta_h/\beta_t = 0.2$, the passing particles' contribution is about 40% higher. This is quite different from fishbone instability in conventional tokamaks, where the mode is driven mainly by either trapped or passing particles.

4. Nonlinear dynamics of beam-driven fishbone: mechanism of chirping

Here we investigate nonlinear evolution of chirping fishbone and associated dynamic behaviour of particles near resonances. The purpose is to understand the chirping mechanism of beam-driven fishbone in spherical tokamaks. Figure 6 shows

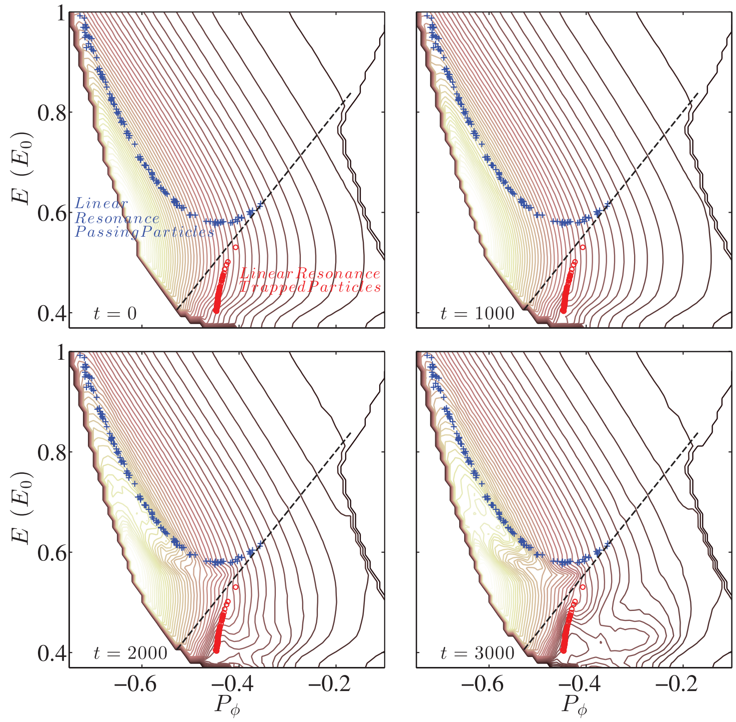

Figure 9. Distribution function at $t = 0,\ 1000,\ 2000$ and 3000 τ_0 with $\mu \simeq 0.467$.

the nonlinear evolution of fishbone for a relatively low linear growth rate case with $\beta_h/\beta_t = 0.2$, and $q_{\min} = 1.321$. The calculated linear mode frequency and growth rate is $\omega = 0.13\ (\omega_0)$ and $\gamma\tau_0 = 0.005$ respectively. The figure shows time evolution of (*a*) *cos* component of U, here U is the stream function of the incompressional part of the perturbed plasma velocity, (*b*) mode frequency, (*c*) total energy changes of passing particles and trapped particles (positive means losing energy), and (*d*) ratio of the energy changes between trapped and passing particles. We observe that the mode saturates around $t \sim 1600\ \tau_0$ and the mode amplitude persists thereafter. Correspondingly, the mode frequency chirps down strongly from $\omega = 0.13\ (\omega_0)$ to $\omega = 0.06\ (\omega_0)$. Interestingly, about half of the frequency drop occurs before the initial saturation. We also observe that, although the passing particle drive (measured by energy change) is initially somewhat larger than that of trapped particles, the trapped particle drive becomes increasingly more important and dominant from $t \sim 1000\ \tau_0$. This indicates that the chirping mode is driven mainly by trapped particles in the nonlinear phase. In addition to mode saturation and frequency chirping, the mode structure also changes significantly as shown in figure 7. We observe that the mode structure evolves from ballooning in the linear phase to anti-ballooning with a broader (2, 1) component in the nonlinear phase.

The corresponding beam ion distribution evolution is shown in figures 8 and 9 in 1D and 2D phase spaces at $t = 0,\ 1000,\ 2000$ and 3000 τ_0 respectively. Clearly, there is a large flattening region induced by both trapped and passing particles. Figure 8 shows the flattening region of the distribution function expands outwards/inwards radially (or in P_ϕ space) in time for trapped/passing particles. For trapped particles, the center of the flattening region also moves from core to edge as the mode chirps down. Figure 9 shows the 2D distribution function in P_ϕ and E space, which clearly presents some details of the distribution change in the nonlinear phase. At $t = 1000\ \tau_0$, when the mode amplitude is small, the perturbation mainly appears around the resonance line shown in figure 5, which proves the main resonances are $p = 0$ and $p = 1$ (as mentioned in the previous section). At $t = 2000$ and 3000 τ_0, around $E \simeq 0.4\ (E_0)$, which corresponds to trapped particles, the distribution function is flattened from the resonance line to the edge. For distribution around $E \sim 0.55\ (E_0)$ to $E \sim 0.8\ (E_0)$, which corresponds to passing particles, the distribution function is flattened from the resonance line to the core. This expansion of flattened region can be understood by dynamics of resonant particles interacting with a chirping mode as shown below.

We now analyze the dynamics of resonant and non-resonant particles interacting with a chirping fishbone in order to understand the mechanism of fishbone nonlinear evolution including frequency chirping. First, we examine the dependence of particle resonance frequency as a function of E and P_ϕ at $\mu \simeq 0.467$. Figure 10(*a*) shows the locations of $p = 0$ and $p = 1$ resonance for three mode frequencies including the linear fishbone frequency of $\omega \simeq 0.13\ (\omega_0)$ and two nearby frequencies. Note that the resonant location does not correspond to smooth lines because it is obtained from particle simulation with a narrow range of μ values. To see the dependence of resonance frequency more clearly, figure 10(*b*) plots $p = 0$ resonant frequency (or precessional drift frequency) of

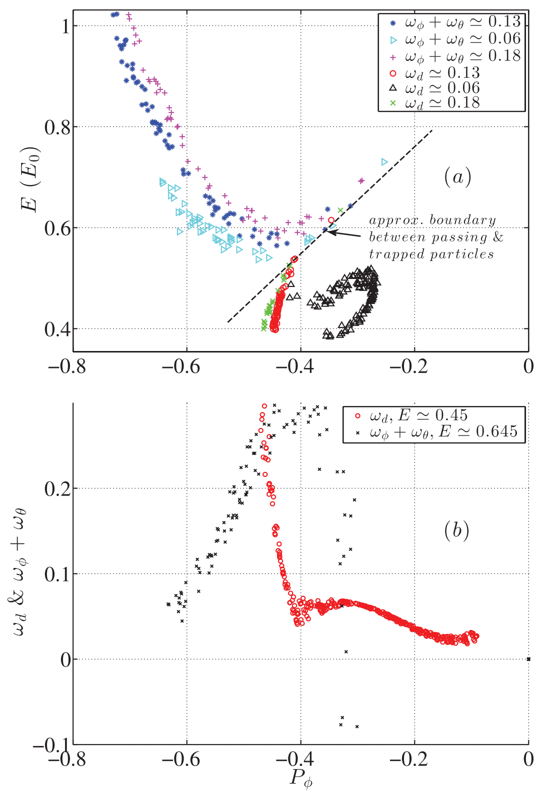

Figure 10. (a) unperturbed trapped and passing resonance particles and near resonance particles in P_ϕ and E phase spaces with $\mu \simeq 0.467$. (b) unperturbed particles frequency versus P_ϕ with $\mu \simeq 0.467$.

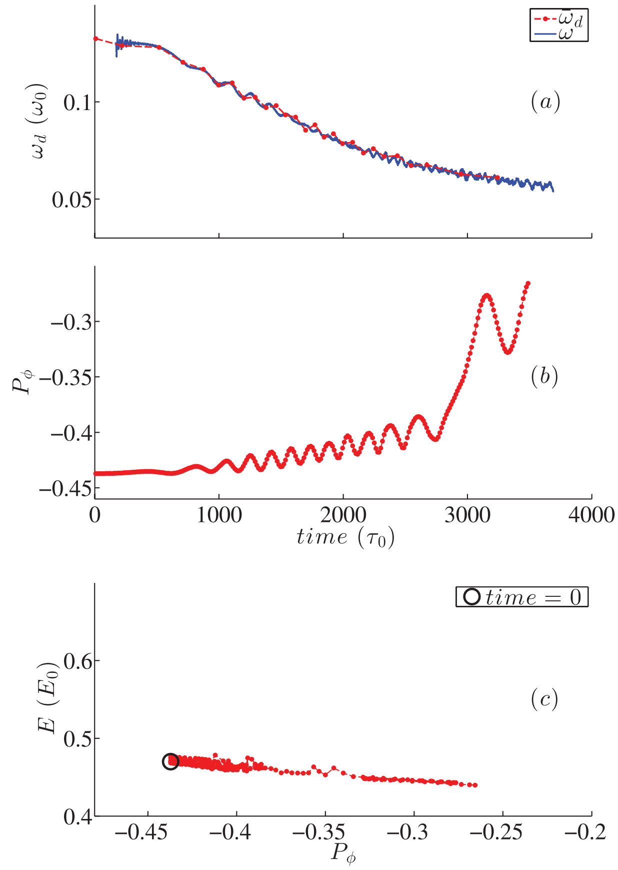

Figure 11. Nonlinear dynamic of a typical trapped particle with $\omega_{d,t=0} \simeq \omega_{\text{linear}}$: (a) mode frequency, and ω_d; (b) P_ϕ versus time; (c) the particle's trajectory in P_ϕ and E spaces.

trapped particles and $p = 1$ resonant frequency of passing particles as a function of P_ϕ at energy values of $E \simeq 0.45$ (E_0) and $E \simeq 0.64$ (E_0) respectively. We observe that the precessional frequency firstly decreases with P_ϕ strongly for $P_\phi < -0.4$, and then changes very slowly for $P_\phi > -0.4$. On the other hand, the $p = 1$ resonance frequency of passing particles increases strongly with P_ϕ for $P_\phi < -0.4$. We will soon show that these different behaviours of resonant frequency are important to the understanding of the dynamics of trapped and passing particles interacting resonantly with the mode.

Figure 11 shows the evolution of precessional drift frequency ((a), red line), P_ϕ (b) and trajectory of a typical resonant trapped particle which is initially in resonance with the fishbone. The mode frequency evolution is also shown ((a), blue line). We observe that the particle keeps in resonance as the mode frequency chirps down. Correspondingly the particle moves outward radially as P_ϕ increases and energy decreases. The movement of particles in the (E, P_ϕ) phase space can be understood from the relationship [36]

$$\frac{\mathrm{d}P_\phi}{\mathrm{d}t} = -\frac{n}{\omega}\frac{\mathrm{d}E}{\mathrm{d}t}. \tag{3}$$

This equation means that the change of particle toroidal angular momentum is proportional to the change of particle energy in the presence of a perturbation with frequency ω and toroidal mode number n. Since P_ϕ can be regarded as a radial variable, this means that a particle moves out radially with decreasing energy. The oscillation of P_ϕ in plot (b) indicates that the particle is trapped in the fishbone mode. The averaged value of P_ϕ increases at such rate that precessional frequency keeps in resonant with the chirping mode. We observe that almost all of these linear resonance trapped particles are phase-locked with the mode. Here we plot only one of them to keep the plot clear. It is instructive to note that there is a big jump in P_ϕ and its oscillation amplitude at $t \sim 2800\ \tau_0$ and $P_\phi \sim -0.4$. This is due to the sudden change of the slope of function $\omega_d(P_\phi)$ near $P_\phi = -0.4$ (see in figure 10). It should be noted that these phase-locking resonant particles cause the radial expansion of beam ion redistribution as mode frequency chirps down (see figure 8).

We now examine the behaviour of non-resonant trapped particles. Figure 12 shows the evolution of precessional drift frequency ((a), red and green lines), P_ϕ (b) and trajectory (c) of two typical non-resonant trapped particles with precessional frequencies less than the initial fishbone frequency. Similarly, figure 13 shows evolution of precessional drift frequency ((a), red and green lines), P_ϕ (b) and trajectory (c) of two typical non-resonant trapped particles with precessional frequencies larger than the initial fishbone frequency. We observe that in

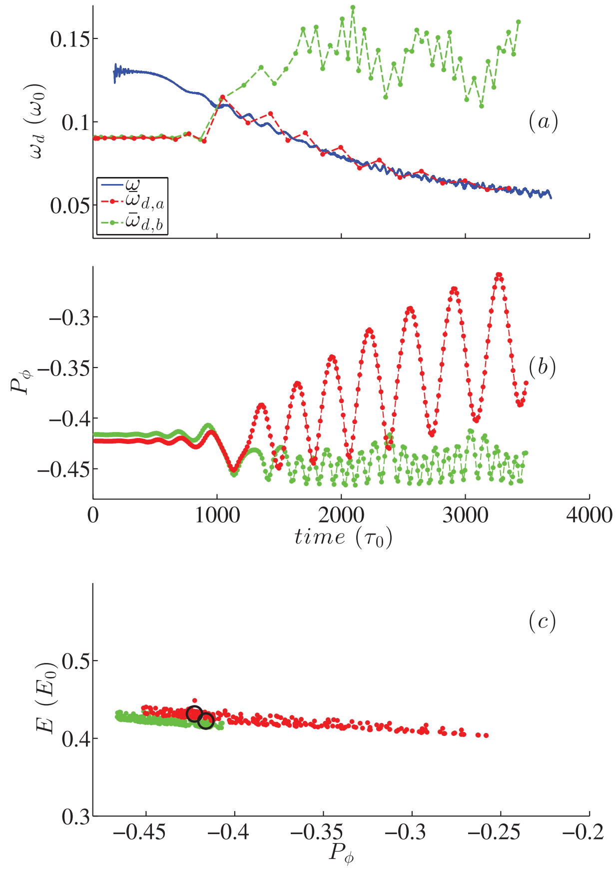

Figure 12. Nonlinear dynamic of trapped particles with $\omega_{d,(t=0)} \simeq 0.7\omega_{\text{linear}}$. Red and green markers present two typical nonlinear resonance particles respectively.

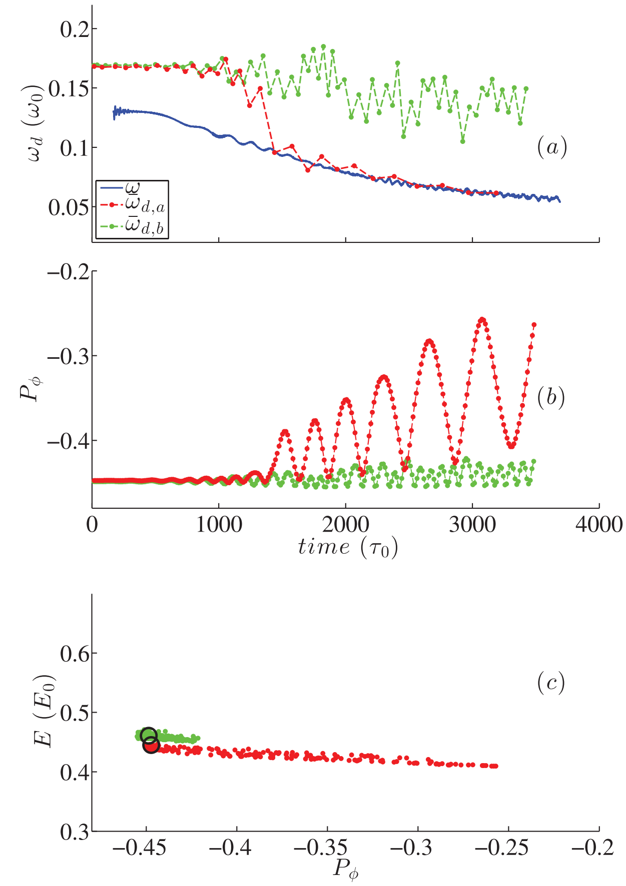

Figure 13. Nonlinear dynamic of trapped particles with $\omega_{d,(t=0)} \simeq 1.3\omega_{\text{linear}}$.

both cases some initially non-resonant trapped particles can become resonant before mode saturation and stay in resonance with the mode as the frequency chirps down.

We now look at the behaviour of resonant passing particles. Figure 14 shows nonlinear dynamics for two typical passing particles with initial frequency $\omega_{\phi,(t=0)} + \omega_{\theta,(t=0)} \simeq \omega_{\text{linear}}$. For orbit *a* (red lines), the particle keeps in resonance with the mode while the averaged P_ϕ decreases as the mode frequency chirps down. The direction of P_ϕ change is different from that of resonant trapped particles due to the opposite slopes of particle frequencies (see figure 10). As a result, the particle gets energy from the mode, in other words, it damps the mode nonlinearly. For orbit *b* (green lines), initially, the particle is in resonance. As the mode frequency chirps, the particle does not lock to the wave phase, in contrast, its frequency slightly increases, while energy decreases. At the end, it oscillates in a small range of P_ϕ and E space, but it still contributes energy to the mode on average.

Figure 15 shows the fraction of phase-locked particles versus initial particle frequency. Here the phase-locked particles include all the particles that are in resonance with the mode near the end of simulation ($t = 3500$) whether they are initially resonant or not. Numerically the ration is defined $\kappa \equiv N_r(\omega_{p,t=0})/N(\omega_{p,t=0})$, where $N_r(\omega_{p,t=0})$ is the number of phase-locking particles with $|\omega_p(t = 3500) - \omega(t = 3500)| < 0.01$ in $\omega_{p,t=0}$ space, and $N(\omega_{p,t=0})$ is the number of total particles in $\omega_{p,t=0}$ space. For trapped particles, $\omega_p = \omega_d$, and for passing particles, $\omega_p = \omega_\phi + \omega_\theta$.

We observe that for particle frequency between 0.15 (ω_0) and 0.06 (ω_0) the majority of trapped particles are phase-locked, while less than half of passing particles keep in resonance with the mode. This indicates that the main mode drive in the nonlinear phase comes from trapped particles. Furthermore, for either trapped or passing particles, a substantial fraction of initially non-resonant particles become resonant and thus play a significant role in mode nonlinear drive and frequency chirping.

Now we can connect the nonlinear dynamics of a single particle's orbit, distribution function and the mode together. For trapped particles, as the frequency chirps down, most of the linear resonant and near resonant particles are phase-locked with the wave, and they move radially and drive the mode continuously, which leads to distribution evolution in the phase space. Meanwhile the mode structure becomes broader at the low field side.

For passing particles, there are also a fraction of particles which keep in resonance nonlinearly. Due to the opposite slopes of the particle frequencies in P_ϕ space, they move from edge to core, and get energy from the mode. But there are

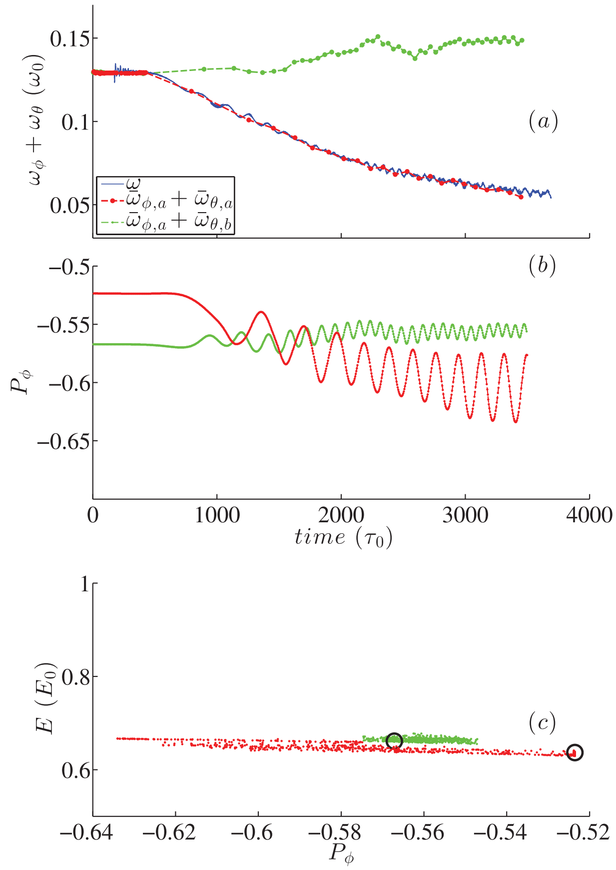

Figure 14. Nonlinear dynamic of passing particles with $\omega_{\phi,(t=0)} + \omega_{\theta,(t=0)} \simeq \omega_{\text{linear}}$.

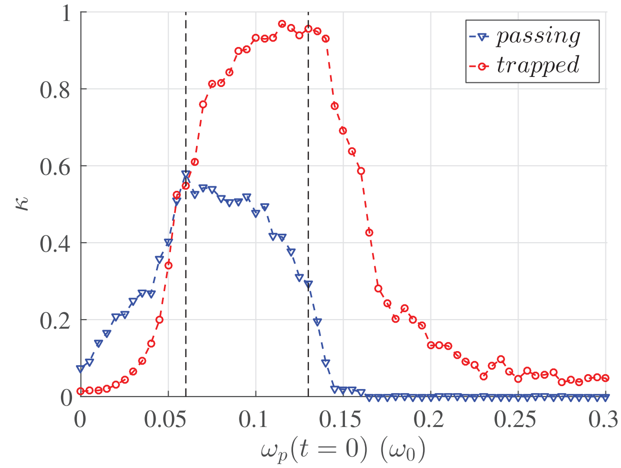

Figure 15. $\kappa \equiv \frac{\text{Phase locked particle number}}{\text{Total particle number}}$ after the mode saturated as a function of the initial particle's frequency.

more particles near resonance that are not phase-locked with the mode. They instead move from core to edge and drive the mode. These particles do not drive the mode continuously like trapped particles, but as the mode frequency chirps down and the resonance line for passing particles moves inwards, more and more particles can become resonant with the mode and drive the mode nonlinearly. Trapped particles provide the dominant nonlinear driving force since the nonlinear driving trapped particles are phase-locked, and they increase in number as frequency chirps down and the mode amplitude grows.

It is instructive to compare our results of fishbone chirping and particle dynamics with the Berk–Breizman hole/clump theory of bump-on-tail instability [30, 31]. The theory shows that a hole/clump structure in distribution can develop from a near-threshold energetic particle-driven instability and the mode frequency chirps up/down while the hole/clump structure moves in phase spaces. Our results are consistent with the Berk–Breizman theory with respect to frequency chirping and associated resonant particle dynamics. In particular, our analysis shows that the resonant particles are trapped by the mode and thus they keep in resonance with the mode as frequency chirps down. Furthermore, a substantial fraction of initially non-resonant particles become resonant as the mode grows and frequency chirps down. This suggests the formation of islands of resonant particles moving in phase spaces as frequency chirps down. Our estimate shows that the adiabatic parameter $\alpha \equiv \frac{d\omega}{\omega_b^2 dt} \leqslant 0.005$ is very small (where ω_b is the bounce frequency of a resonant particle trapped in the mode). This indicates that the adiabatic assumption of the Berk–Breizman theory is valid for our case.

It should be noted however that our results also differ from that of Berk–Breizman theory in important ways. The simulated evolution of beam ion distribution does not show a clear local hole/clump structure moving in phase spaces. Instead the beam ion redistribution is fairly global. This is probably due to large oscillation of P_ϕ of resonant particles or large phase space island. It can be shown that a large island size can result from weak gradient of $\omega_d(P_\phi)$ as shown in figure 10. Specifically an equation of motion for a resonant particle trapped in the finite amplitude fishbone mode can be derived to show that the corresponding oscillating amplitude of P_ϕ is inversely proportional to $\sqrt{|d\omega_d/dP_\phi|}$. Thus the width of phase space island of resonant trapped particles is larger for smaller gradient of $\omega_d(P_\phi)$. Finally our results show that the mode structure changes significantly during the nonlinear evolution. This effect might affect the mode chirping and beam ion redistribution. However, this effect was not included in the Berk–Breizman theory.

5. Summary

In summary, linear and nonlinear simulations of $n = 1$ fishbone have been carried out for the first time for the parameter regime of NSTX with low aspect ratio, high beta, high sheared rotation, and $q_{\min} > 1$. This parameter regime is very different from that of moderate aspect ratio, low beta, and small rotation of conventional tokamaks. The simulation is self-consistent with evolving mode structure in the nonlinear regime. This spherical tokamak parameter regime leads to new features of fishbone with respect to linear stability and nonlinear evolution. The main results are listed below:

(1) Linearly, the fishbone is driven by both trapped particles and passing particles. For a realistic distribution function from NBI, the instability drive of passing particles is comparable to that of trapped particles. This is quite different from the classical fishbone in conventional tokamaks, where the fishbone is mainly driven by either trapped or passing particles. The significant passing particle contribution is likely induced by a finite precession drift frequency due to low aspect ratio and high beta.
(2) The effects of rotation are destabilizing and a new instability region appears at higher $q_{\min}$. It is shown that the sheared rotation affects the sound-Alfveń continuum significantly, which can in turn lead to modification of mode stability.
(3) The mode saturates nonlinearly due to flattening of distribution function, and it persists after initial saturation while mode frequency chirps down in such a way that the resonant trapped particles move out radially and keep in resonance with the mode. Correspondingly the flattening region of beam ion distribution expands radially outward. There is no apparent hole/clump structure as in the Berk–Breizman model because of large oscillating amplitude in P_ϕ of resonant particles phase-locked with the fishbone.
(4) A substantial fraction of initially non-resonant trapped particles become resonant and keep in resonance with the mode as the mode grows and frequency chirps down. On the other hand, the fraction of resonant passing particles is significantly smaller than that of trapped particles. Indeed our analysis shows that trapped particles provide the main drive in the nonlinear phase.

Acknowledgments

This work is supported by the Department of Energy Scientific Discovery through Advanced Computing (SciDAC) under Grant No. DE-AC02-09CH11466, the National Natural Science Foundation of China under Grant No. 11505022, China Postdoctoral Science Foundation under Grant No. 2014M561218, and the CASHIPS Director's Fund under Grant No. YZJJ201510. All this simulations were performed on super-computers at the National Energy Research Scientific Computing Center (NERSC). One of the authors (Feng Wang) thanks Dr. Huishan Cai from University of Science and Technology of China), Dr. Mario Podesta, Dr. Eric Fredrickson and Dr. Nikolai Gorelenkov from Princeton Plasma Physics Laboratory for their valuable suggestions. And we also thank Dr. Guangzhou Hao from University of California, Irvine for his help about NSTX experimental data.

References

[1] McGuire K. *et al* 1983 *Phys. Rev. Lett.* **50** 891–5
[2] Chen L. *et al* 1984 *Phys. Rev. Lett.* **52** 1122–5
[3] Coppi B. and Porcelli F. 1986 *Phys. Rev. Lett.* **57** 2272–5
[4] Heidbrink W.W. *et al* 1986 *Phys. Rev. Lett.* **57** 835–8
[5] Heidbrink W.W. and Sager G. 1990 *Nucl. Fusion* **30** 1015–25
[6] Nave M.F.F. *et al* 1991 *Nucl. Fusion* **31** 697–710
[7] von Goeler S. *et al* 1996 *Rev. Sci. Instrum.* **67** 473
[8] Kass T. *et al* 1998 *Nucl. Fusion* **38** 807–19
[9] Fredrickson E., Chen L. and White R. 2003 *Nucl. Fusion* **43** 1258–64
[10] Chen W. *et al* 2010 *Nucl. Fusion* **50** 084008
[11] Toi K. *et al* 2000 *Nucl. Fusion* **40** 1349–62
[12] Betti R. and Freidberg J.P. 1993 *Phys. Rev. Lett.* **70** 3428–30
[13] Wang S.J. 2001 *Phys. Rev. Lett.* **86** 5286–8
[14] Fredrickson E.D. *et al* 2014 *Nucl. Fusion* **54** 093007
[15] Fredrickson E.D. *et al* 2015 *Phys. Plasmas* **22** 032501
[16] Park W. *et al* 1999 *Phys. Plasmas* **6** 1796
[17] Fu G.Y. *et al* 2006 *Phys. Plasmas* **13** 052517
[18] Breslau J.A., Jardin S.C. and Park W. 2007 *Phys. Plasmas* **14** 056105
[19] Lang J.Y., Fu G.Y. and Chen Y. 2010 *Phys. Plasmas* **17** 042309
[20] Brennan D.P. *et al* 2012 *Nucl. Fusion* **52** 033004
[21] Cheng C.Z. and Chance M.S. 1987 *J. Comput. Phys.* **71** 124–46
[22] Breslau J.A. *et al* 2011 *Nucl. Fusion* **51** 063027
[23] Fu G.Y. 2012 M3D-K simulations of beam-driven Alfvén modes in DIII-D *54th Annual Meeting of the American Physical Society Division of Plasma Physics (Providence, Rhode Island, 29 October–2 November 2012)* invited talk, paper JI2.00003 (http://meetings.aps.org/Meeting/DPP12/Content/2392c)
[24] Cai H.S. and Fu G.Y. 2012 *Phys. Plasmas* **19** 072506
[25] Deng W.J. and Fu G.Y. 2014 *Comput. Phys. Commun.* **185** 96–105
[26] Shen W. *et al* 2014 *Phys. Plasmas* **21** 092514
[27] Shen W. *et al* 2015 *Phys. Plasmas* **22** 042510
[28] Liu D. *et al* 2015 *Phys. Plasmas* **22** 042509
[29] Cai H.S. and Fu G.Y. 2015 *Nucl. Fusion* **55** 022001
[30] Berk H.L., Breizman B.N. and Petviashvili N.V. 1997 *Phys. Lett.* A **234** 213
[31] Berk H.L. *et al* 1999 *Phys. Plasmas* **6** 3102
[32] Wang F. *et al* 2013 *Phys. Plasmas* **20** 102506
[33] Wang F. *et al* 2013 *Phys. Plasmas* **20** 072506
[34] Pankin A. *et al* 2004 *Comput. Phys. Commun.* **159** 157–84
[35] Hao G.Z. *et al* 2015 Effect of low frequency MHD instability on fast ion distribution in NSTX *57th Annual Meeting of the APS Division of Plasma Physics (Savannah, Georgia, 16–20 November 2015)* (http://meetings.aps.org/Meeting/DPP15/Content/3000)
[36] White R.B. *et al* 2010 *Plasma Phys. Control. Fusion* **52** 045012